RSC Advances

PAPER

View Article Online
View Journal | View Issue

Cite this: *RSC Adv.*, 2017, **7**, 27840

Effect of hydrogen on dislocation structure and strain-induced martensite transformation in 316L stainless steel

Sang Hwan Bak,[a] Sung Soo Kim[b] and Dong Bok Lee*[c]

Received 24th January 2017
Accepted 10th May 2017

DOI: 10.1039/c7ra01053b

rsc.li/rsc-advances

Hydrogen embrittlement behavior with respect to strain-induced martensite (SIM, α') and the dislocation structure in 316L stainless steel were investigated using tensile testing at strain rates of 2×10^{-6} to 2×10^{-2} s^{-1} at room temperature. The deformed specimens with and without hydrogen were examined using MFM, neutron diffraction, TEM, and a Feritscope. The results showed that ductility, tensile stress, and hardness increased with decreasing strain rate and an increasing amount of SIM. Hydrogen caused SIM to be distributed locally in a α'/γ laminated structure. The H-free sample had a larger quantity of SIM than the H-charged sample at the same plastic strain. Hydrogen changed the dislocation structure from only cellular to a mixed structure comprising both cellular and planar dislocations. H-charged 316L SS had a diffuse reflection, which implied that short-range ordering formed during tensile testing. It was concluded that hydrogen induced planar dislocation and suppressed SIM formation, leading to cleavage fracture and softening.

Introduction

Hydrogen embrittlement (HE) is a critical issue in the welding, processing, and corrosion of metals. Many hypotheses have been proposed to account for HE. Among these, it has been postulated that HE results from the build-up of high internal stress concentrations due to the difficulty of cross-slip,[1–4] the occurrence of brittle fractures due to hydrogen-enhanced plasticity,[5–7] and decohesion of the grain boundary in hydrogen environments.[8,9] However, these explanations cannot be applied to austenitic stainless steel because the role of strain-induced martensite (SIM, α') has not been considered. Regarding HE in austenitic stainless steels, the characteristics of SIM remain controversial due to the discrepant findings. It has been reported that the formation of SIM promotes HE because SIM provides a diffusion path for hydrogen, leading to a decrease in cohesive energy at grain boundaries.[10–12] In contrast, hydrogen has been shown to suppress SIM formation[13] and accelerate the transformation of SIM into austenite.[14]

In this study, room-temperature (RT) tensile tests were conducted on H-free and H-charged 316L austenitic stainless steel (SS) at strain rates of 2×10^{-6} to 2×10^{-2} s^{-1} to clarify the mechanism underlying changes in ductility caused by SIM. The amount of SIM in H-free and H-charged 316L SS was measured *in situ* during the RT tensile tests. The volume fraction and SIM distribution were measured for deformed 316L SS to identify the mechanism of the suppression of SIM formation in H-charged 316L SS. The change in dislocation structure and the transition from ductile to brittle fractures caused by hydrogen were investigated by transmission electron microscopy (TEM).

This study aimed to investigate (1) the effect of hydrogen on the distribution and amount of SIM formation in 316L SS, (2) the effect of strain-induced disordering on the mechanical properties, such as strain rate dependence, and (3) the effect of planar dislocation and ordering on fracture behavior.

Experimental

Materials and hydrogen charging

316L SS, which has a composition of Fe–16.7Cr–10.2Ni–2.0Mo–1.1Mn–0.6Si–0.5Cu–0.2Co–0.03P–0.02C–0.003N–0.001S (wt%), was solution-annealed at 1100 °C for 1 h and quenched in water. The microstructure of 316L SS was examined by optical microscopy after etching with $H_2O : HF : HNO_3$ solution (8 : 1 : 1, vol%) for 5 min, and its grain size was measured using the intercept method. Hydrogen charging was performed using electrolytic charging for 20 h at 80 °C with a current density of 500 A m^{-2} using 1 N H_2SO_4 solution containing 0.25 g L^{-1} $NaAsO_2$. The amount of hydrogen in 316L SS was analyzed with a hydrogen analyzer (LECO RH-404) using five independent samples.

Quantification of SIM and tensile tests

RT tensile tests were conducted on H-free and H-charged 316L SS at strain rates of 2×10^{-6} to 2×10^{-2} s^{-1} immediately after

[a]*Functional Materials Research Team, Advanced Materials & Processing Centre, Institute for Advanced Engineering, South Korea*
[b]*Korea Atomic Energy Research Institute, South Korea*
[c]*School of Advanced Materials Science and Engineering, Sungkyunkwan University, South Korea. E-mail: dlee@skku.ac.kr*

hydrogen charging. Tests were performed twice on rod-shaped specimens with a diameter of 4 mm and a gauge length of 25.4 mm, and mean values were calculated. During testing, the amount of SIM was measured *in situ* using a Feritscope (Fisher MP30). After calibrating the Feritscope using the standard sample, the average amount of SIM formed was measured either *ex situ* on the fracture surface five times, or *in situ* at the center of the gauge section. The values measured using the Feritscope were in agreement with those measured using magnetic force microscopy (MFM) when the dependence of strain rate on the amount of martensite was considered. The volume fraction and distribution of SIM on the surface were measured in deformed samples after tensile tests using MFM by applying the distinct magnetic properties of nonmagnetic austenite (γ) and ferromagnetic α'.[15–17] MFM and atomic force microscopy (AFM) images were obtained in air using a scanning probe microscope in tapping/lift mode with a lift height of 100 nm.

Observation of short-range ordering (SRO) and dislocation structure

Changes in the lattice parameters of 316L SS after tensile tests were determined using neutron diffraction (ND). ND data were collected using a high-resolution powder diffractometer (HRPD) over the 2Θ range of 0–160° with a step size of 0.05° and a wavelength (λ) of 1.83429 Å. The data were refined using the Rietveld method and FullProf software by changing the peak positions with a confidence level of $\Delta d/d = 0.004\%$.[18] After tensile tests, thin foil specimens were examined using transmission electron microscopy (TEM) at 200 kV to examine the dislocation structure and diffuse peaks generated by SRO formation along the [111], [110], and [112] zone axes.

Results and discussion

Hydrogen diffusion and microstructure

Fig. 1 shows the optical microstructure of the H-charged 316L SS with a grain size of 57 ± 6 μm. The amount of hydrogen immediately after hydrogen charging was 39 ± 2 ppm, which was less than the 56–75 ppm previously obtained under similar charging conditions from samples with grain sizes of 130–300 μm.[19–21] Hydrogen discharges rapidly in material with fine grains. As the density of grain boundaries decreases with decreasing equivalent hydrogen pressure ($P_{H_2}^{eq.}$), the hydrogen-discharging rate increases with decreasing hydrogen solubility.[21,22] Notably, hydrogen diffusion along grain boundaries was shown to be enhanced by several orders of magnitude when the grain size was a few tens of micrometers.[23]

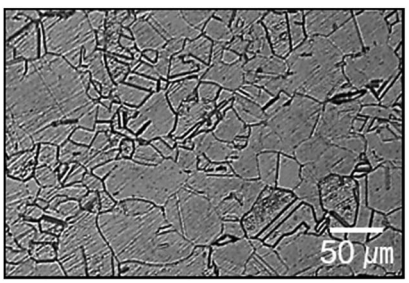

Fig. 1 Optical microstructure of H-charged 316L SS.

Hydrogen was generally confined to the surface during charging. According to diffusion eqn (1) for 316L SS at 25–960 °C,[20] the hydrogen diffusion coefficient was measured as 7.2 × 10^{-15} m^2 s^{-1} at a hydrogen charging temperature of 80 °C.

$$D = 6.2 \times 10^{-3} \exp\left(-\frac{53\,630}{RT}\right) \quad (1)$$

where, D is the diffusion coefficient of hydrogen (m^2 s^{-1}), R is the gas constant (J K^{-1} mol^{-1}), and T is the temperature (K). The penetration depth of hydrogen, d, can be roughly expressed by eqn (2).

$$d = \sqrt{2Dt} \quad (2)$$

When D was 7.2 × 10^{-15} m^2 s^{-1} and the charging time (t) was 20 h, d became 32 μm, which was considerably smaller than 4 mm (the sample diameter). Hydrogen was apparently confined near the surface. Although the center of the specimen was H-free before tensile tests, the transgranular (TG) brittle fractures occurred in the H-charged 316L SS, and cleavage was evident across the sample after tensile test.

Effect of hydrogen on tensile properties and fracture mode

The mechanical properties strongly depended on the strain rate and sensitivity to the tensile stress, ductility, hardness, and strain hardening. Strain hardening is defined as (TS − YS)/YS, where TS and YS are the tensile and yield stresses, respectively. However, the yield stress displayed a positive strain rate sensitivity regardless of hydrogen content (Fig. 2a). The effect of hydrogen varied with the strain rate. H-Charging decreased the tensile stress, ductility, hardness, and strain hardening, but slightly increased the yield stress, except at the slowest strain rate (Fig. 2b–d), which was consistent with previous reports of the tensile properties of H-charged austenitic stainless steels.[24–26] The decrease in the strain hardening by hydrogen, especially at a strain rate of 2 × 10^{-6} s^{-1}, was in agreement with reported hydrogen-induced softening after hydrogen charging and tensile testing under similar conditions.[20]

Fig. 3 shows the fracture surfaces of H-free and H-charged 316L SS after RT tensile testing. H-free samples displayed ductile fractures with fine dimples and coalescent voids or cavities at all strain rates (Fig. 3a and b). Void formation and coalescence under an applied tensile stress are known to result from ductile fracture.[27] The nucleation of voids is associated with the type of defect in the crystal.[28–30] In contrast, the fracture mode of H-charged samples changed from mixed fractures, with dimples and cleavages, at a strain rate of 2 × 10^{-2} s^{-1} (Fig. 3c) to enhanced brittle fractures, characterized by cleavages across the surface, at a strain rate of 2 × 10^{-6} s^{-1} (Fig. 3d). Cleavage fractures became more pronounced with decreasing strain rate. In particular, parallel cracks developed with a rectilinear shape (Fig. 3d). As hydrogen

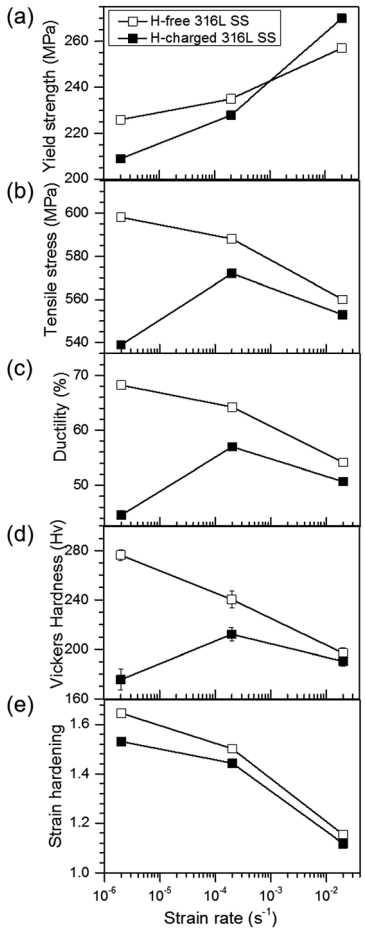

Fig. 2 Mechanical values of H-free and H-charged 316L SS as a function of strain rate. (a) Yield stress, (b) tensile stress, (c) ductility, (d) Vickers microhardness, and (e) strain hardening.

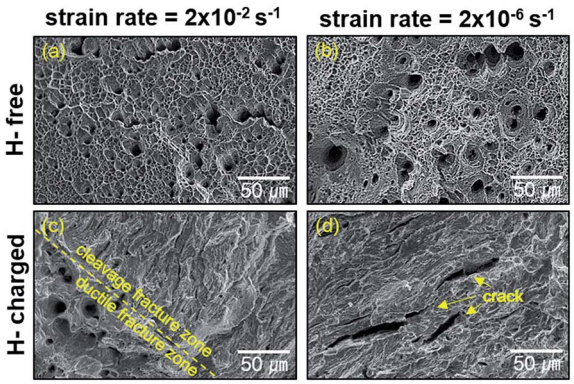

Fig. 3 Fracture surface of 316L SS after tensile testing. (a) H-Free (strain rate = 2×10^{-2} s^{-1}), (b) H-free (strain rate = 2×10^{-6} s^{-1}), (c) H-charged (strain rate = 2×10^{-2} s^{-1}), (d) H-charged (strain rate = 2×10^{-6} s^{-1}).

clearly induced brittle fracture with cleavage, the reduction in elongation by hydrogen charging in the H-charged 316L was attributed to the transition from ductile to brittle fracture modes.[30] Furthermore, as SIM increased the ductility (Fig. 2) and H-free samples displayed uniform ductile fractures with fine dimples and voids irrespective of strain rates (Fig. 3a and b), brittle fractures might be controlled by inhibition of the γ–α transformation.

Effect of hydrogen on SIM formation

Fig. 4a shows the amount of SIM formed on the fracture surface relative to the strain rate. With decreasing strain rate, the amount of SIM increased in the H-free sample, but decreased in the H-charged sample. The amount of SIM was greater in H-free samples than in H-charged samples at the same strain rates. The amount of SIM was lowest in the H-charged sample at the lowest strain rate of 2×10^{-6} s^{-1}, which suggested that hydrogen suppressed SIM formation during tensile testing. To confirm this, SIM was measured *in situ* using a Feritscope in H-free and H-charged samples during tensile tests at a strain rate of 2×10^{-6} s^{-1}. The amount of formed SIM was controlled by the plastic deformation and the presence of hydrogen (Fig. 4b). The largest decrease in SIM occurred at a strain of 35–40% between H-free and H-charged samples. This showed clearly that hydrogen evidently suppressed SIM formation, even with the same amount of plastic deformation.

To investigate the effect of hydrogen on the volume fraction and distribution of SIM formed, H-free and H-charged 316L SS were examined before and after tensile testing using MFM and an image analyzer (Fig. 5). In the MFM images, the dark and light phases corresponded to martensite (α′) and austenite (γ), respectively. These phases were more clearly discernable in the image analyzer images. Before tensile testing, the average amount of SIM was 1.5%, with SIM regions aligned along the tensile axis, tens to hundreds of micrometers apart (Fig. 5a). The amount of SIM increased with increasing strain, irrespective of the presence of hydrogen. In the H-free sample, SIM was distributed uniformly (Fig. 5b). However, in the H-charged sample, SIM was distributed locally in the α′/γ laminated structure with stacking intervals of several tens of micrometers (Fig. 5c). As localized cracking occurred at the interface of α′/γ,[6,21,28] hydrogen changed the distribution of SIM in the α′/γ laminated structure, leading to a lower resistance to cracking. The suppression of SIM formation by hydrogen during tensile testing, as shown in Fig. 4b, was a plausible cause of the loss in ductility. It is reasonable that SIM formation is beneficial for the

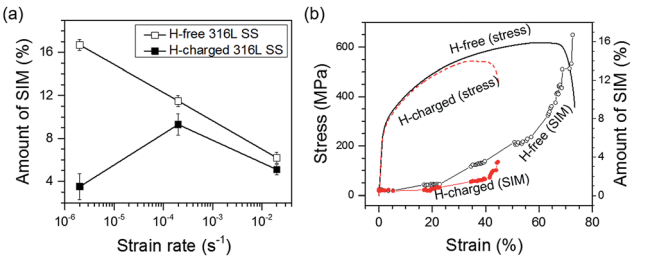

Fig. 4 (a) Amount of strain-induced martensite as a function of the strain rate on H-free and H-charged 316L SS after tensile tests. (b) Stress and amount of SIM formed as a function of strain on H-free and H-charged 316L SS at a strain rate of 2×10^{-6} s^{-1}.

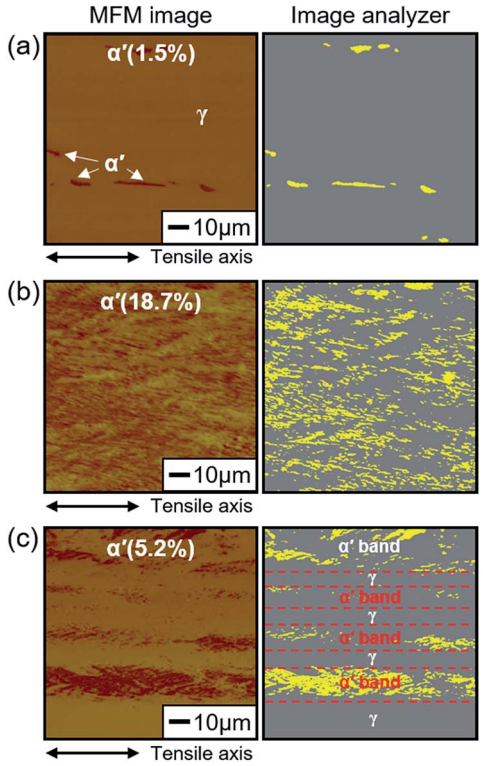

Fig. 5 Distribution of austenite and martensite in 316L SS at a strain rate of 2×10^{-6} s^{-1} after fracture. (a) Before tensile test (strain, 0%), (b) H-free, and (c) H-charged.

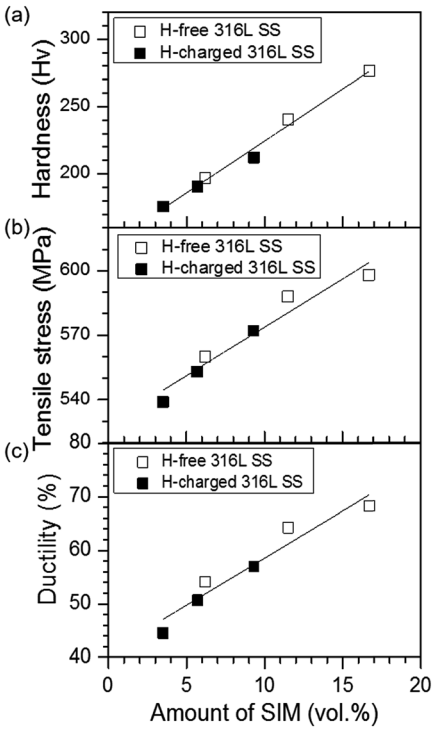

Fig. 6 Linear dependence of (a) microhardness, (b) tensile stress, and (c) ductility on the amount of SIM formed in H-free and H-charged 316L SS after tensile testing.

various mechanical properties of 316L SS. The enhanced brittle fracture at a low strain rate in the H-charged sample, as shown in Fig. 3, was related to decreased SIM formation during tensile deformation. As explained later, the decrease in microhardness owing to hydrogen softening in the H-charged sample provided further strong evidence that hydrogen suppresses SIM formation.

SIM and strain-rate dependence of mechanical properties

The relationship between the amount of SIM and the mechanical properties is depicted in Fig. 6. The microhardness, tensile stress, and ductility of H-free and H-charged 316L SS were positively correlated with the amount of SIM formed during RT tensile testing. SIM beneficially increased hardness, tensile stress, and ductility, regardless of the absence or presence of hydrogen. The tensile properties of the H-free sample were dependent on the strain rate (Fig. 2 and 6), which was also related to the amount of SIM formed during plastic deformation. The hardness of the H-free sample increased with increasing SIM amount. This implied that SIM was harder than austenite.[32] Transformation-induced plasticity (TRIP) similarly increased ductility and tensile stress through deformation-induced martensite transformation.[33,34] The reason for the dependence of strain-rate on the amount of SIM formed in austenitic stainless steel (Fig. 4a) and the enhancement of ductility by the hard SIM (Fig. 6) was unclear. The linear relationship shown in Fig. 6 demonstrates that SIM formation significantly affected the mechanical properties of H-free and H-charged 316L SS. The dependence of mechanical properties on the amount of SIM (Fig. 6) and the suppression of the SIM formation by hydrogen (Fig. 4b and 5) indicated that hydrogen decreased the amount of SIM formed during tensile testing, which led to losses in ductility and tensile stress.

To investigate the changes in the lattice parameters of H-free 316L SS during RT tensile testing, the *d*-spacing of austenite and martensite was determined by neutron diffraction. The variation in *d*-spacing was defined as the fractional change in the position of austenite (111) and martensite (110) before and after tensile testing. Fig. 7 shows that the *d*-spacing of (110) martensite increased with decreasing strain rate. In contrast, the *d*-spacing of austenite (111) decreased with decreasing strain rate, indicating that the lattice in austenite had contracted slightly. This strain rate dependence suggested that a time-dependent process was involved in SIM formation. A similar result has also been observed in 304 SS[24] and TRIP steels.[31,34]

As ductility depended on the strain rate in 304 and 316L SS with SIM, and in 310 SS without SIM,[35] the formation of SIM cannot fully explain the strain-rate dependence of the ductility of austenitic stainless steels. As the disordered phase had lower yield stresses, and higher ductility and strain hardening than the ordered phase,[36,37] SIM formed in 316L SS likely corresponded to the disordered phase, which also formed in 310 SS due to dislocation movement during RT tensile testing.[38,39] When plastic deformation occurs in an austenitic alloy, strain-

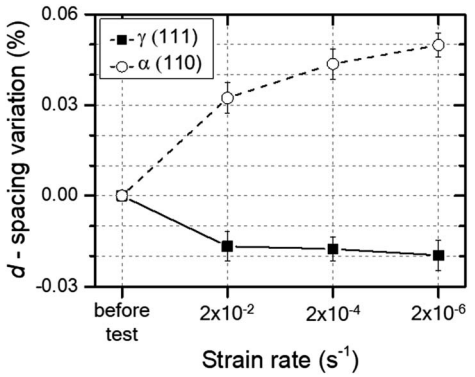

Fig. 7 Variation of *d*-spacing as a function of the strain rate for austenite and martensite in H-free 316L SS.

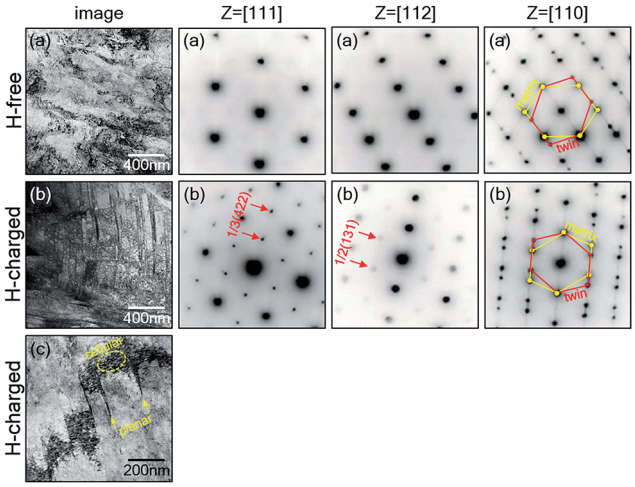

Fig. 8 Bright-field TEM images and selected area electron diffraction (SAED) patterns of 316L SS after RT tensile tests at a strain rate of 2×10^{-6} s^{-1}. (a) H-Free, (b) H-charged, (c) H-charged and 10% tensile deformed.

induced disordering (SID) results from formation of a disordered phase or destruction of the ordered phase due to moving dislocations.[40] In contrast, the disordered phase was formed predominantly by plastic deformation when the rate of disordering exceeded the rate of strain-induced ordering (SIO).[41] Therefore, SIM corresponded to the disordered phase, because ductility and strain hardening increased linearly with an increasing amount of SIM (Fig. 6). Fig. 7 provides further supporting evidence, indicating that martensite expanded the lattice, the magnitude of which increased with decreasing strain rate. In summary, we suggest that the dependence of strain rate on the mechanical properties of 316L SS can be reasonably explained by disordered SIM formation during plastic deformation, and hydrogen promoted strain-induced ordering (SIO) due to hydrogen suppressing SIM formation.

Effect of hydrogen on dislocation structure

To evaluate the effect of hydrogen on the dislocation structure and SRO formation during plastic deformation, we conducted TEM analysis of 316L SS after tensile testing and on 10% deformed 316L SS. Twinning occurred along the [110] zone axis in H-free and H-charged 316L SS. The H-free sample showed only cellular dislocation, and no diffuse reflections were present in the SAED pattern because no SRO formed (Fig. 8a). The H-charged sample showed a mixed dislocation structure and diffuse 1/3{422} and 1/2{131} reflections along the zone axes of [111] and [112], respectively, which implied that SRO formed during tensile testing (Fig. 8b). Diffuse reflections were also observed in other austenitic alloys, such as alloy 600 under slow strain rate tests in water at 360 °C,[42] hydrogenated 310 SS deformed at RT,[7] and Fe–Mn–Al alloy after tensile deformation at −200 °C.[43] To observe mixed dislocations during the initiation stage of plastic deformation, 10% deformed H-charged 316L SS was investigated (Fig. 8c). Mixed dislocations comprising both planar and cellular dislocations were observed. Indeed, cellular dislocations existed between planar dislocations, which were distributed several hundred nanometers apart parallel to each other in a rectilinear shape. Planar dislocation is a characteristic feature of ordered structures.[44] Moreover, it suppresses local cross-slip, which was hampered by SRO, leading to a loss of ductility.[27,44] The above observation provides strong evidence that the cause of hydrogen embrittlement in 316L SS was hydrogen-mediated SRO formation.

The cleavage fractures shown in Fig. 3c and d can also be explained by SRO formation. Generally, long-range ordering (LRO) formed in the alloys fractures intergranularly,[27,44] and makes twinning very difficult.[43] For example, in Fe_3Si and Fe_3Al alloys, twinning did not occur in the fully ordered state, which displayed an IG fracture,[45] but occurred in the short-range ordered state, which displayed TG or IG + TG fractures at less than ~10 at% Si concentrations.[27,45] Moreover, high- and low-angle grain boundaries in the ordered state provide an easy path for nucleation and/or propagation of cracks.[45] The change in brittle fracture from TG to IG was therefore related to the increase in degree of order. That is, the nucleation and/or propagation of cracks could be generated along low- and high-angle grain boundaries when SRO and LRO formed in the alloy, respectively.

It is well known that 316L SS forms ordered phases, such as Ni_3Fe, NiFe, and Fe_3Ni, with relatively strong binding forces.[46] Although multiple ordering processes took place among Ni, Fe, and Cr atoms during the formation of ordered phases, the LRO phase did not form because of the non-stoichiometric chemical composition of 316L SS and interference by other elements, such as carbon. Therefore, in this study, only the formation of an SRO phase was considered in 316L SS. TG fracture (cleavage) occurred in H-charged 316L SS because cracks were grew easily along low-angle grain boundaries due to SRO formation during plastic deformation.

Conclusions

RT tensile tests were conducted on H-free and H-charged 316L SS to investigate the effect of hydrogen on the strain-rate dependence of the mechanical properties, SIM formation,

dislocation structure, and fracture mode. The strain-rate dependence of ductility was due to strain-induced disordering, indicating that a disordered phase (SIM) formed upon plastic deformation. Hydrogen suppressed SIM formation during plastic deformation, and SIM was distributed locally in the α'/γ laminated structure at stacking intervals of several tens of micrometers, leading to cracking. As SIM was beneficial to the mechanical properties of 316L SS, the loss in ductility and hydrogen softening in the H-charged 316L SS were attributed to hydrogen suppressing SIM formation. This was considered the main cause of hydrogen embrittlement in austenitic stainless steels. Therefore, the two major factors leading to brittle fracture in H-charged 316L SS are the restriction of cross slip by planar dislocations, and the suppression of strain-induced disordering by hydrogen.

Acknowledgements

This work was supported by the "Development of the High-Efficiency Low-Emission Future Energy Production Technology (EO15580)" project of the National Research Council of Science & Technology (NST) grant by the Korean government (MSIP) (No. CRC-15-07-KIER). Special thanks are due to B. An who conducted MFM experiments at the National Institute of Advanced Industrial Science and Technology (AIST).

Notes and references

1 C. A. Zapffe and C. E. Sims, *Trans. AIME*, 1941, **145**, 225.
2 F. Garofalo, Y. T. Chou and V. Ambegaokar, *Acta Metall.*, 1960, **8**, 504.
3 B. A. Bilby and J. Hewitt, *Acta Metall.*, 1962, **10**, 587.
4 D. Pérez Escobar, C. Miñambres, L. Duprez, K. Verbeken and M. Verhaege, *Corros. Sci.*, 2011, **53**, 3166.
5 H. K. Birnbaum and P. Sofronis, *Mater. Sci. Eng., A*, 1994, **176**, 191.
6 J. Song and W. A. Curtin, *Acta Mater.*, 2014, **68**, 61.
7 J. Konrad, S. Zaefferer, A. Schneider, D. Raabe and G. Frommeyer, *Intermetallics*, 2005, **13**, 1304.
8 N. Takano, *Key Eng. Mater.*, 2010, **417–418**, 285.
9 V. Olden, C. Thaulow and R. Johnsen, *Mater. Des.*, 2008, **29**, 1934.
10 G. Han, J. He, S. Fukuyama and K. Yokogawa, *Acta Mater.*, 1998, **46**, 4559.
11 C. L. Briant, *Metall. Trans. A*, 1979, **10**, 181.
12 T. P. Perng and C. J. Altstetter, *Metall. Trans. A*, 1987, **18**, 123.
13 Y. Mine, Z. Horita and Y. Murakami, *Acta Mater.*, 2009, **57**, 2993.
14 V. M. Shyvaniuk, Y. Mine and S. M. Teus, *Scr. Mater.*, 2012, **67**, 979.
15 L. Zhang, B. An, S. Fukuyama, T. Iijima and K. Yokogawa, *J. Appl. Phys.*, 2010, **108**, 063526.
16 A. Miller, Y. Estrin and X. Z. Hu, *Scr. Mater.*, 2002, **47**, 441.
17 J. Sort, A. Concustell, E. Menéndez, S. Suriñach, M. D. Baró, J. Farran and J. Nogués, *Appl. Phys. Lett.*, 2006, **89**, 032509.
18 S. K. Das, P. R. Okamoto, P. M. J. Fisher and G. Thomas, *Acta Metall.*, 1973, **21**, 913.
19 I. Aubert, J. M. Olive and M. Saintier, *Mater. Sci. Eng., A*, 2010, **527**, 5858.
20 A. M. Brass and J. Chene, *Corros. Sci.*, 2006, **48**, 3222.
21 A. Oudriss, J. Creus, J. Bouhattate, C. Savall, B. Peraudeau and X. Feaugas, *Scr. Mater.*, 2012, **66**, 37.
22 J. Yao and J. R. Cahoon, *Acta Metall. Mater.*, 1991, **39**, 119.
23 J. H. Austin, T. S. Elleman and K. Verghese, *J. Nucl. Mater.*, 1973, **48**, 307.
24 Y. S. Kim, S. H. Bak and S. S. Kim, *Metall. Mater. Trans. A*, 2016, **47**, 222.
25 H. J. Ji, I. J. Park, S. M. Lee and Y. K. Lee, *J. Alloys Compd.*, 2014, **598**, 205.
26 C. San Marchi, B. P. Somerday, X. Tang and G. H. Schiroky, *Int. J. Hydrogen Energy*, 2008, **33**, 889.
27 M. J. Marcinkowski, M. E. Taylor and F. X. Kayser, *J. Mater. Sci.*, 1975, **10**, 406.
28 M. J. Marcinkowski, *Electron Microscopy and Structure of Materials*, ed. G. Thomas, R. M. Fulrath and R. M. Fisher, University of California Press, Berkeley, 1972, p. 382.
29 C. D. Beachem, *Fracture*, ed. H. Liebowitz, Academic Press, New York, 1968, vol. 1, p. 243.
30 S. H. Bak, M. A. Abro and D. B. Lee, *Metals*, 2016, **6**, 169.
31 L. Zhang, Z. Li, J. Zheng, Y. Zhao, P. Xu, C. Zhou and X. Li, *Int. J. Hydrogen Energy*, 2013, **38**, 8208.
32 K. Spencer, J. D. Embury, K. T. Conlon, M. Veron and Y. Brechet, *Mater. Sci. Eng., A*, 2004, **387**, 873.
33 I. Tamura, *Met. Sci.*, 1982, **16**, 245.
34 J. K. Hwang, I. H. Son, J. Y. Yoo, A. Zargaran and N. J. Kim, *Met. Mater. Int.*, 2015, **21**, 815.
35 G. W. Form and W. M. Baldwin, *Trans. ASME*, 1956, **48**, 474.
36 N. S. Stoloff and R. G. Davies, *Acta Metall.*, 1964, **12**, 473.
37 M. J. Marcinkowski and D. S. Miller, *Philos. Mag.*, 1961, **6**, 871.
38 V. Gerold and H. P. Karnthaler, *Acta Metall.*, 1989, **37**, 2177.
39 N. Clement, D. Caillard and J. L. Martin, *Acta Metall.*, 1982, **32**, 961.
40 P. B. Littlewood, *Phys. Rev. B: Condens. Matter Mater. Phys.*, 1986, **34**, 1363.
41 Y. S. Kim, W. Y. Maeng and S. S. Kim, *Acta Mater.*, 2015, **83**, 507.
42 D. P. Abraham and C. J. Altstetter, *Metall. Trans. A*, 1995, **26**, 2859.
43 K. Sato, M. Ichinose, Y. Hirotsu and Y. Inoue, *ISIJ Int.*, 1989, **29**, 868.
44 S. M. L. Sastry and H. A. Lipsitt, *Metall. Trans. A*, 1977, **8**, 1543.
45 M. J. Marcinkowski. *Treatise on materials science and technology*, ed. H. Herman, Academic Press Inc., New York, 1977, vol. 5, p. 181.
46 S. S. Kim, S. H. Kang and Y. S. Kim, *Korean J. Met. Mater.*, 2016, **54**, 154.